

1 Absorption cross sections and local mode analysis for neopentane

2 Peter Bernath^{a,b}, Edwin L. Sibert III^c, Keith LaBelle^b, Jianbao Zhao^d, Brant Billinghurst^d

3 ^aDepartment of Chemistry and Biochemistry, Old Dominion University, VA, USA, 23529

4 ^bDepartment of Physics, Old Dominion University, VA, USA, 23529

5 ^cDepartment of Chemistry and Theoretical Chemistry Institute, University of Wisconsin-Madison,
6 Madison, Wisconsin, USA 53706

7 ^dCanadian Light Source Far-Infrared Beamline, 44 Innovation Blvd, Saskatoon, Canada SK S7N
8 2V3

9 *Corresponding author: pbernath@odu.edu

10

11 **Highlights**

- 12 • High resolution absorption spectra of neopentane, C(CH₃)₄
- 13 • Cross sections for neopentane broadened by N₂
- 14 • Measurements performed for 203-294 K
- 15 • Useful for analysis of spectra of Titan

16

17

18

19 **Abstract**

20 Spectra of neopentane, 2,2-dimethylpropane, C(CH₃)₄, were recorded in the 1200-1650 cm⁻¹
21 region by high resolution Fourier transform spectroscopy at the Canadian Light Source (CLS) and
22 converted to absorption cross sections. Samples were at 203, 233, 266 and 294 K with 0, 10, 30
23 and 100 Torr of nitrogen broadening gas. The previously published cross sections in the CH
24 stretching region (2550-3350 cm⁻¹) [JQSRT **251**, 107034 (2020)] were recalibrated and checked
25 with two additional spectra recorded at Old Dominion University in the 1000-5000 cm⁻¹ region.
26 Local mode calculations for the CH stretching modes were carried and interactions with the
27 overtones of the CH₂ scissor vibrations were needed to obtain agreement with experiment.

28

29 **Introduction**

30 Neopentane (2,2-dimethylpropane, C₅H₁₂) belongs to a class of small hydrocarbons that includes
31 methane, tetrahedrane [1] and adamantane [2] with tetrahedral symmetry. Although these
32 molecules have no dipole moment, they have characteristic sharp Q-branches in their infrared
33 vibrational spectra which aids in their detection. Small hydrocarbons such as methane and ethane
34 are present in many planetary atmospheres including Earth [3], the giant planets [4] and
35 particularly Titan [5], a moon of Saturn. Larger hydrocarbons such as benzene are formed by

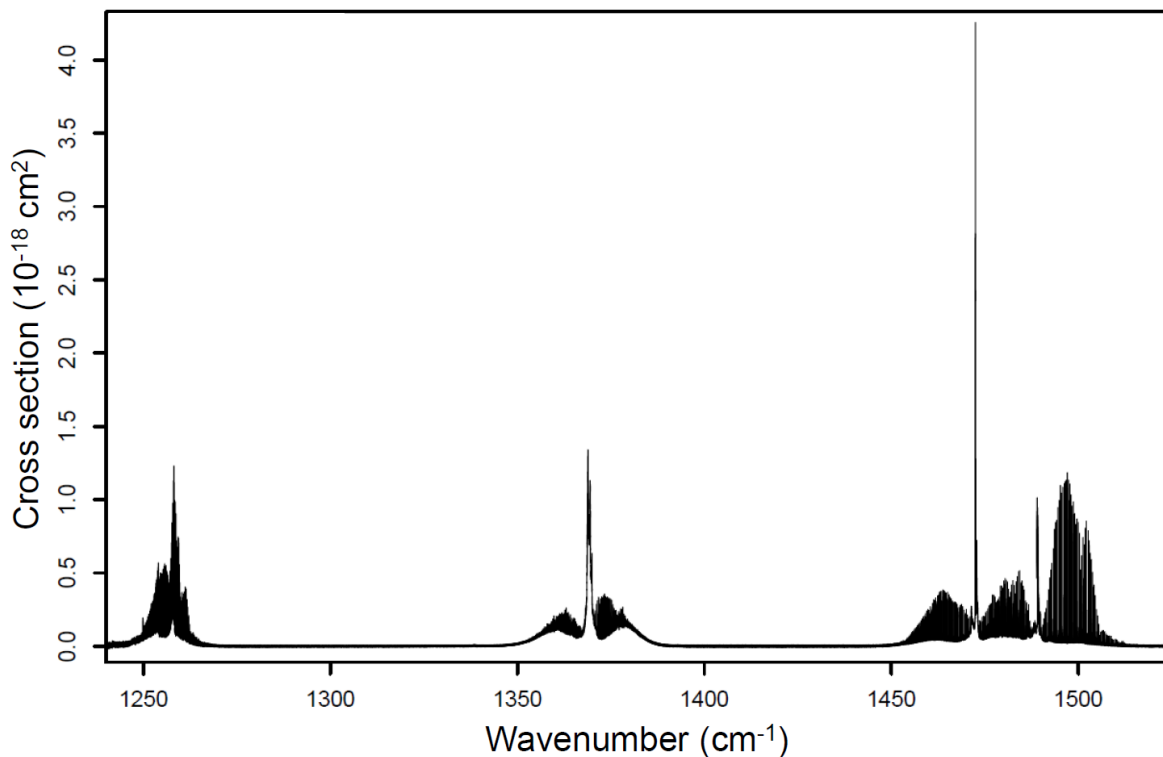
36 photochemistry and ion molecule chemistry in the upper atmosphere of Titan [6]. Neopentane is
37 potentially present on Titan but infrared absorption cross sections are required for detection.

38 There has already been considerable work on the infrared and Raman spectra of neopentane [7-
39 11] as well as calculations of vibrational structure [12-13]. Recently we recorded high resolution
40 spectra in the 800-1600 cm^{-1} region and carried out local mode calculations to interpret the
41 observations [14]. In a second paper, infrared absorption cross sections in the 2550-3350 cm^{-1}
42 region were reported with nitrogen as a broadening gas [15], but the local mode analysis for the
43 CH stretching modes was not published at that time. In this third paper, we now present high
44 resolution absorption cross sections for the 1200-1650 cm^{-1} region with nitrogen as the broadening
45 gas. The absorption cross sections reported in paper two were recalibrated and two additional
46 spectra were recorded covering the 1000-5000 cm^{-1} region to check this recalibration. In addition,
47 the local mode analysis was extended to cover the CH stretching region and used to interpret the
48 spectra.

49 Neopentane has 45 normal modes and 19 fundamental frequencies of vibration, 3 of a_1 symmetry
50 (ν_1 - ν_3), 1 a_2 (ν_4), 4 e (ν_5 - ν_8), 4 t_1 (ν_9 - ν_{12}) and 7 t_2 (ν_{13} - ν_{19}), of which only the t_2 modes are infrared
51 active [13, 14]. In the 1200-1650 cm^{-1} region there are just 3 infrared active fundamental modes:
52 ν_{17} (t_2) 1256.7 cm^{-1} , ν_{16} (t_2) 1369.4 cm^{-1} and ν_{15} (t_2) 1472.471 cm^{-1} [14]. There are 5 fundamental
53 vibrational frequencies in the 2800-3000 cm^{-1} region: $\nu_1(a_1)$, 2909 cm^{-1} ; $\nu_4(e)$, 2955 cm^{-1} ; $\nu_9(t_1)$,
54 (2942) cm^{-1} ; $\nu_{13}(t_2)$, 2959.6 cm^{-1} ; $\nu_{14}(t_2)$, 2876.2 cm^{-1} , but only 2 are infrared active [14].

55 **Experimental method**

56 High resolution infrared spectra of neopentane, pure and broadened by nitrogen, were recorded at
57 the Canadian Light Source (CLS) Far Infrared Beamline with a Fourier transform spectrometer,
58 similar to our previous work, e.g., [15,16]. Figure 1 is an overview spectrum of neopentane at
59 203.5 K from 1240 to 1520 cm^{-1} . A 2-m base-path White-type cell with KBr windows was used
60 with a nominal path length of 8 meters at 4 temperatures and 3 N_2 broadening gas pressures (plus
61 the pure sample): 203, 233, 266 and 294 K and 10, 30 and 100 Torr of broadening gas (total
62 pressures). The samples were prepared by adding a small amount of neopentane to the cell, then
63 adding the broadening gas and recording the total pressure. Pressures were measured with three
64 recently calibrated Baratron pressure gauges (Model 127AA up to 1 Torr, Model 627B up to 10
65 Torr and Model 626B up to 1000 Torr). An SP Scientific model RC211 refrigerated re-circulating
66 methanol bath cooled the cell. The cell temperature was monitored with 4 wire PT100 RTD
67 (platinum resistance temperature detector) sensors with an estimated accuracy of ± 2 K.



68

69 **Figure 1:** Overview absorption cross sections of neopentane at 203.5 K.

70 The CLS spectrometer was a Bruker IFS 125 HR Fourier transform instrument with a KBr
 71 beamsplitter, internal globar source, a 1200-1680 cm^{-1} band pass filter and a liquid N_2 -cooled
 72 narrow band MCT (HgCdTe) detector. The spectral resolution varied depending on the total
 73 pressure: 0.0014 cm^{-1} (pure sample), 0.003 cm^{-1} (10 Torr), 0.01 cm^{-1} (30 Torr), and 0.04 cm^{-1} (100
 74 Torr). The background spectra were recorded at 0.01536, 0.048, 0.048 and 0.048 cm^{-1} resolution,
 75 respectively, and Fourier interpolated to match the higher resolution spectra. The pressure and
 76 temperature parameters used for the samples are shown in Table 1. The cell was evacuated and
 77 refilled for each spectrum. For each spectrum, a minimum of 400 interferograms (200 forward and
 78 200 backward) were co-added and boxcar apodization (i.e., no apodization) was used with a zero-
 79 filling factor of at least 8.

80

81

82

83

84

85

86

87

88 Table 1. Experimental conditions for each spectrum.

Temp (K)	Neopentane (Torr)	Total (Torr)	Temp (K)	Neopentane (Torr)	Total (Torr)
203.55	0.0248	0.0248	266.25	0.0901	0.0901
203.55	0.0254	10.1	266.15	0.1056	10.2
203.55	0.0443	30.1	266.15	0.1647	30.0
203.55	0.0450	100.2	266.15	0.2705	100.7
Temp (K)	Neopentane (Torr)	Total (Torr)	Temp (K)	Neopentane (Torr)	Total (Torr)
232.95	0.0492	0.0492	293.65	0.1105	0.1105
232.95	0.0545	10.2	293.75	0.1666	10.2
232.85	0.0526	30	293.85	0.2161	30.0
232.95	0.0543	100.3	293.75	0.3012	101.5

89

90 The CLS transmission spectra are converted to cross sections using [17]:

$$91 \quad \sigma(\nu, T) = -\frac{10^4 k_B T}{Pl} \ln \tau(\nu, T)$$

92 in which $\tau(\nu, T)$ is the transmittance at wavenumber ν (cm^{-1}) and temperature T (K), P is the
 93 pressure of the absorbing gas in pascals (Pa), l is the optical path length (m), and k_B is the
 94 Boltzmann constant (1.380649×10^{-23} J/K). The path length used to calculate the cross sections was
 95 8.63 m (including the total distance of 63 cm from the cell windows to the White cell mirrors).
 96 Residual water absorption lines were removed by hand.

97 The wavenumber calibration was carried out with an N_2O sample using reference line positions
 98 from the HITRAN database [18]. The calibration factor of 1.000000352(14) was applied to all
 99 spectra, which amounts to a shift of about 0.00045 cm^{-1} near 1300 cm^{-1} . After calibration, the
 100 wavenumber scale is accurate to better than 0.0001 cm^{-1} .

101 Cross sections for the CH stretching region were reported previously [15]. Based on spectra
 102 recorded at ODU, the pressure-pathlength was erroneously divided by a factor of 3. This factor of
 103 3 has been removed and the cross sections have been recalculated.

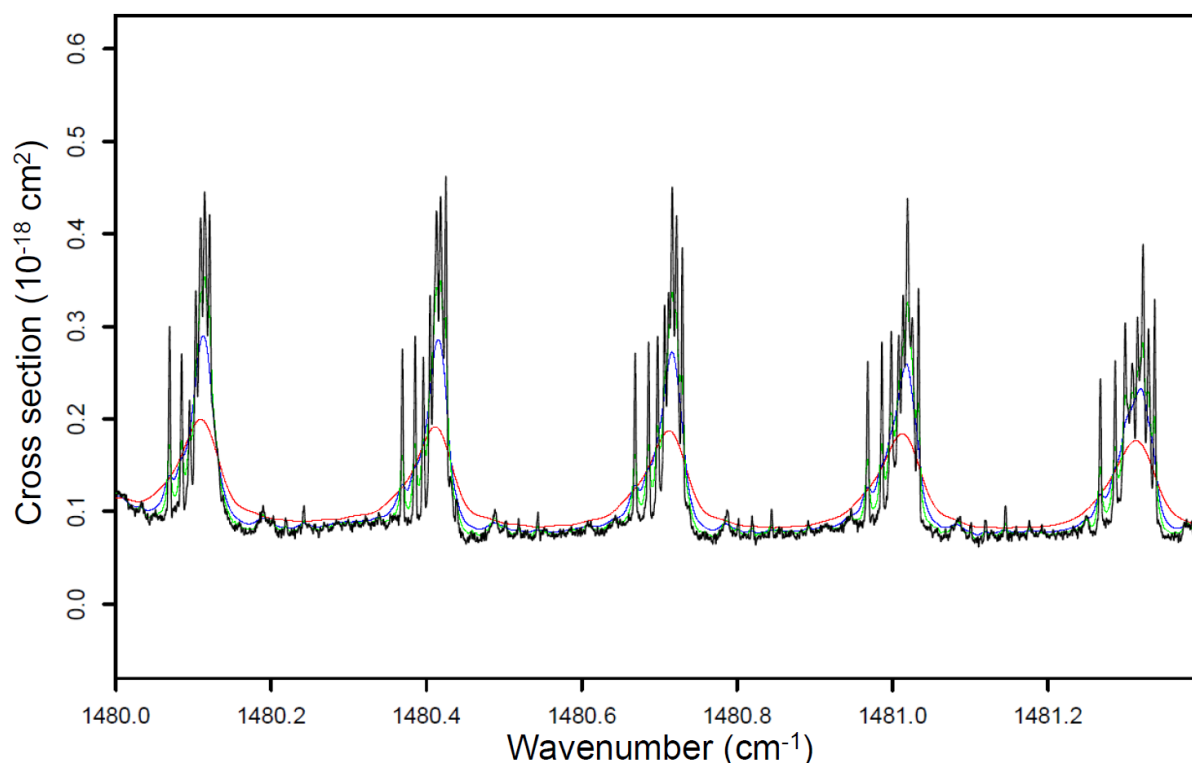
104 The 16 infrared absorption cross section files for neopentane are available for the $1200\text{-}1650 \text{ cm}^{-1}$
 105 region along with the 16 recalibrated files for the $2550\text{-}3350 \text{ cm}^{-1}$ region from the MoLLIST
 106 (Molecular Line Lists, Intensities and SpecTra) [19] web site
 107 <http://bernath.uwaterloo.ca/molecularlists.php>. Each cross section value (in $\text{cm}^2/\text{molecule}$) needs
 108 to be multiplied by 10^{-18} .

109

110

111 Results, Local Mode Analysis and Discussion

112 For the 1200-1650 cm^{-1} region (Figure 1), the 16 new CLS neopentane spectra improve on the
113 resolution and reach a lower temperature than the two ODU (Old Dominion University) spectra of
114 pure samples analyzed previously [14]. The effect of the nitrogen broadening on the spectral
115 features is illustrated in Figure 2. Each of these P lines is made up of a number of features due to
116 “cluster” splitting from the partial lifting of the K degeneracy as the molecule rotates [20]. These
117 cluster splittings are much clearer in the new spectra (Figure 2) and we have started a rotational
118 analysis [21].



119

120 **Figure 2.** A portion of the P branch of the ν_{15} (t_2) mode of neopentane at 203.5 K showing the
121 cluster splittings and the effect of broadening by N_2 (black, pure neopentane; green, 10.1 Torr; blue,
122 30.1 Torr; and red, 100.2 Torr).

123 In addition to the spectra recorded at the CLS, two additional spectra were recorded at ODU to
124 check on the recalibration of the cross sections in the CH region. The 1000-5000 cm^{-1} region was
125 covered at a resolution 0.05 cm^{-1} with an MCT detector, a KBr beamsplitter, a Ge filter and a
126 globar source. The 19.75-cm long cell with KBr windows was at 294 K and then cooled to 217 K
127 for the second spectrum. The two ODU spectra were converted to cross sections and calibrated
128 with the new room temperature cross sections recorded at the CLS. The 2660-3070 cm^{-1} region
129 was then integrated and the areas were 60.1 $\text{cm}/\text{molecule}$ (294 K) and 59.6 $\text{cm}/\text{molecule}$ (217 K)

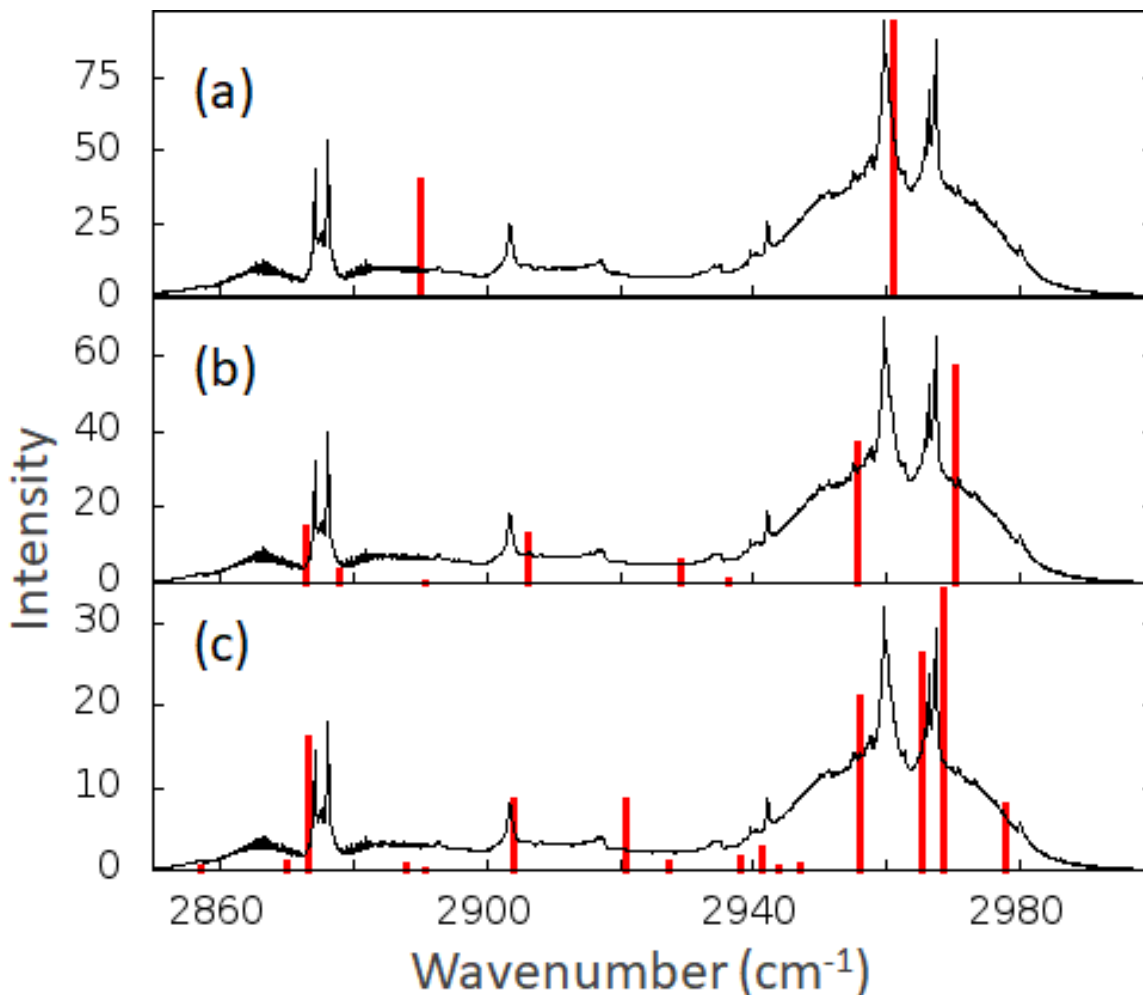
130 cm/molecule compared to the average of 56.6 ± 0.6 cm/molecule for the recalibrated spectra. The
131 difference of 5.7% is taken as an estimate of the error in the cross sections for the CH region.

132 The mean and standard deviation of the cross section area of an isolated band between 1335 cm^{-1}
133 and 1400 cm^{-1} is 4.62 ± 0.08 cm/molecule. The estimate of the precision of the cross sections in
134 the lower wavenumber region is therefore about 2%. However, there are no independent
135 measurements for comparison so the overall accuracy is likely about 5-6%, similar to the higher
136 wavenumber region.

137 The CH stretching region is more difficult to analyze than $1200\text{-}1650 \text{ cm}^{-1}$ region: rotational
138 analysis does not seem promising and even the vibrational structure is not clear. The corrected
139 figures from our second paper [15] are provided as Supplementary Information. Only two strong
140 allowed t_2 fundamental bands, $\nu_{13}(t_2)$, 2959.6 cm^{-1} and $\nu_{14}(t_2)$, 2876.2 cm^{-1} , are predicted in the C-
141 H stretching region [14]. Additional bands appear because the overtone and combination bands
142 of the scissors modes have Fermi resonance interactions with the C-H stretching modes [22,23].
143 As presented here, a local mode model that includes these interactions is in much better agreement
144 with experimental observations.

145 The comparison of theory and experiment is shown in Figure 3. The top panel shows the results
146 of a CH stretch only calculation. With the local-mode model the transitions are predicted to occur
147 at 2890.2 and 2961.1 cm^{-1} with intensities of 39.7 and 93.7 km/mol for each of the triplet
148 components of the IR-active t_2 states. The local mode diagonal elements were scaled by 0.961 .
149 The corresponding B3LYP/6-311++(d,p) values from Gaussian [24] are 3009.0 and 3080.1 with
150 intensities of 41.5 and 96.6 km/mol , respectively.

151



152
 153 Figure 3: Comparison of local mode stick spectra (red) to experimental (black) spectrum recorded
 154 at $T = 203$ K for three different levels of theory. (a) neglects Fermi coupling to CH_2 scissors, (b)
 155 neglects Fermi coupling of scissors to other low-frequency modes, and (c) full coupled.

156
 157 The results of Fig. 3(b) are the standard local-mode model results with Fermi couplings to the CH_2
 158 scissors. The results are in qualitative agreement. In order to understand these results we note that
 159 there are 78 combination bands and overtones of scissor states with two quanta of excitation. While
 160 the local-mode Hamiltonian matrix is easy to construct and sparse, since the only anharmonicities
 161 considered are those between states of the individual methyl groups [23], the analysis is difficult
 162 with this many states. For this reason, for our analysis we consider symmetry using a two step
 163 approach.

164 Following our standard approach we write the local-mode Hamiltonian as

165
$$H = H_{str} + H_{sci} + V. \quad (1)$$

166 Here V includes the stretch-scissor Fermi coupling terms that couple the CH stretch states to the
 167 CH_2 scissor overtone and combination modes. H_{str} describes 12 quadratically coupled CH local
 168 modes all with the same frequency; H_{sci} describes 12 quadratically coupled CH_2 scissor vibrations.
 169 At the harmonic level these vibrations all have the same frequency, but the corresponding
 170 overtones are detuned from the combination modes by including a diagonal anharmonicity.
 171 Finally the overtones corresponding to vibrations on the same CH_3 group are allowed to couple
 172 via a Darling-Dennison resonance term. The details of these couplings have been described
 173 previously by Tabor et al. [23].

174 Rather than find the eigenvalues of this Hamiltonian in terms of the local mode basis, we transform
 175 to an intermediate representation in which the basis set is a direct product of the stretch/scissor
 176 eigenstates of H_{str} and H_{sci} , respectively. The eigenvalues of the stretch and scissor Hamiltonians
 177 are found by diagonalizing H_{str} and H_{sci} , respectively. The diagonalization procedure
 178 automatically creates symmetrized states. However, whenever there are degeneracies, one must be
 179 careful to construct the proper linear combination. Linear combinations of the triply degenerate t_2
 180 CH stretch states are carried out so that these triplets of states correspond to the x , y , and z
 181 components. A similar process is carried out for the scissor overtones and combination states. The
 182 anharmonicities included in the local-mode model remove many of the degeneracies, that are
 183 expected based on a harmonic analysis, and this manifold of states breaks up into 8a, 8e, and 18t
 184 states. This result is based on examining the degeneracies in the eigenvalues of H_{sci} .

185 Focusing on those states that are coupled to the t_{2z} IR-active CH stretch states, we find 11 scissor
 186 overtone and combination states that are coupled via the term V in Eq. (1). As the anharmonic
 187 terms in H_{sci} are relatively small, we use the normal mode labels to identify the eigenstates of H_{sci} .
 188 The 12 scissor fundamentals are $\nu_2(a_1)$, $\nu_{10}(t_1)$, $\nu_6(e)$, $\nu_{16}(t_2)$, $\nu_{15}(t_2)$. The first entry in Table 2
 189 corresponds to a state with t_{2z} symmetry which is well-described as a state with two quanta of
 190 excitation in mode 16, a normal mode that has t_2 symmetry. The second column provides select
 191 information about the specific form of how scissor states are constructed to yield the correct overall
 192 t_{2z} symmetry. As an example, the combination state $15(t_2)16(t_2)$ is 9-fold degenerate in the
 193 harmonic limit. The state with t_{2z} symmetry is best described as the specific linear combination
 194 $|1_{15x}1_{16y}\rangle + |1_{15y}1_{16x}\rangle$ where the notation for each of the two basis states has one quantum of
 195 excitation in the modes that are indicated as subscripts. Table 2 also includes the corresponding
 196 energies as well as the couplings to each of the z -components of the two IR-active CH stretch
 197 states. Both V_1 and V_2 matrix elements are found by reexpressing the local mode stretch-bend
 198 Fermi couplings as couplings between the eigenstates of H_{str} and H_{sci} .

199

200

201 Table 2: Scissor combination states and their coupling matrix elements with the t_{2z} CH stretch
 202 states.

203

Symmetry	Basis state	Energy	V_1	V_2
16(t_2)16(t_2)		2721.5	-29.6	0.1
2(a)16(t_2)		2758.1	24.7	0.7
10(t_1)16(t_2)		2806.0	1.0	-9.4
6(e)16(t_2)		2816.4	1.0	6.5
15(t_2)16(t_2)	$ 1_{15x}1_{16y}\rangle$ + $ 1_{15y}1_{16x}\rangle$	2842.7	2.9	4.1
2(a)15(t_2)	$ 1_21_{15z}\rangle$	2878.2	1.9	-6.9
10(t_1)10(t_1)		2889.6	-12.3	-5.9
6(e)10(t_1)	$ 1_{6b}1_{10z}\rangle$	2896.2	-15.9	7.9
10(t_1)15(t_2)	$ 1_{10x}1_{15y}\rangle$ - $ 1_{10y}1_{15x}\rangle$	2921.2	18.1	2.0
6(e)15(t_2)	$ 1_{6a}1_{15z}\rangle$	2932.7	-7.8	-6.3
15(t_2)15(t_2)	$ 1_{15x}1_{15y}\rangle$	2959.6	-5.7	-7.5

204

205

206 Table 2 reports the Fermi couplings V_1 (with state at 2890.2 cm^{-1}) and V_2 (with state at 2961.1 cm^{-1})
207 between the scissor states and the t_{2z} stretch states. Diagonalizing the 13×13 stretch/scissor
208 Hamiltonian, whose elements are given in Table 2 along with the values of diagonal elements
209 given directly above, leads to the same spectral results as diagonalizing the 90×90 local-mode
210 matrix Hamiltonian.

211 At this level of theory and based on the energies of the stretch and scissor states one expects, and
212 indeed one finds that the theoretical high-energy doublet (2955.7/2970.4 cm^{-1}) is well described
213 as a linear combination of the CH stretch state with zero-order energy 2961.1 cm^{-1} and the
214 combination band $|1_{15x}1_{15y}\rangle$ whose zero-order energy is 2960.5 cm^{-1} . The coupling is more
215 complex at lower energies, with several states taking part in the mixing.

216 Although the agreement between theory and experiment is fairly good, in general there appear to
217 be too few transitions predicted by theory. As an example, in the higher energy region, theory
218 predicts a doublet, whereas the experiment shows three intense peaks consisting of a single and
219 doublet at energies 2959.6, 2966.3, and 2976.4 cm^{-1} , respectively. Apparently there are additional
220 mixings at play beyond those considered in our local-mode model.

221 Our earlier analysis of the CH_2 scissor fundamentals [14] points to a possible shortcoming of the
222 model. In that work we found that the $\nu_{15}(t_2)$ band is strongly mixed with a background state. The

223 mixing leads to two equal intensity peaks at 1472.5 cm⁻¹ and 1489.0 cm⁻¹, respectively. Our
 224 calculation revealed that the background state is the combination band of the $\nu_7(e)$ and $\nu_{19}(t_2)$.
 225 The observed fundamentals of these two bands are 1060.0 cm⁻¹ and 418 cm⁻¹, respectively. The
 226 cubic-coupling between the CH₂ scissor and the combination band was calculated numerically at
 227 the B3LYP/6-311++(d,p) level to be -8.7 cm⁻¹ a value consistent with the observed splitting of
 228 16.5 cm⁻¹. Following the notation of Raynes [25], the relevant coupling term is

$$229 \quad V_F = F \left[(S_{15z}S_{19z} - \frac{1}{2}S_{15x}S_{19x} - \frac{1}{2}S_{15y}S_{19y})S_{7a} \right. \\
 230 \quad \left. + \frac{\sqrt{3}}{2}(S_{15x}S_{19x} - S_{15y}S_{19y})S_{7b} \right]. \quad (2)$$

231 There is a typo in our equation with this term in our previous paper [14]. The e_a and e_b were
 232 switched and a $\sqrt{3}$ on the z-component was missed. The subsequent matrix that we wrote down is
 233 correct as are the results. One can use those matrix results to include this Fermi interaction for all
 234 the states in Table 2 with excitation in mode 15. One finds that the state $|1_{6a}1_{15z}\rangle$ is coupled to
 235 the $|1_{6a}1_{7a}1_{19z}\rangle$ with a coupling of $F/\sqrt{8} = -8.7$ cm⁻¹. The highest energy state is more
 236 complicated, since there are two total quanta in mode 15. Here one must consider coupling between
 237 the scissor combination band $|1_{15x}1_{15y}\rangle$ and 7 other states $|1_{15x}1_{7a}1_{19y}\rangle$, $|1_{15x}1_{7b}1_{19y}\rangle$,
 238 $|1_{15y}1_{7a}1_{19x}\rangle$, $|1_{15y}1_{7b}1_{19x}\rangle$, $|2_{7b}1_{19x}1_{19y}\rangle$, $|1_{7a}1_{7b}1_{19x}1_{19y}\rangle$, $|2_{7a}1_{19x}1_{19y}\rangle$. For the
 239 diagonal energies of the 7 latter states we use experimental fundamental excitation energies and
 240 assumed we could sum the energies for the combination bands

241 The modified model increases the Hamiltonian describing the CH stretch region from a 13×13
 242 matrix to a 24×24 matrix. The extra states are the above 7 plus one additional for each of the
 243 four other combination bands with excitation in mode 15. The spectral results are given in Table
 244 3 and shown in Fig. 3. One observes improved agreement throughout the CH stretch spectral
 245 region.

246

247 Table 3: Eigenstates (cm⁻¹) and intensities (km/mol) for the modified local mode Hamiltonian.

248

Energy	Intensity		Energy	Intensity
2715.9	1.3		2903.9	9.5
2754.3	0.9		2921.6	9.0
2806.3	0.3		2928.6	0.6
2816.1	0.2		2937.8	1.9
2832.3	0.2		2941.1	2.8
2857.2	0.5		2950.4	0.1

2869.3	8.6		2956.0	25.5
2871.1	6.7		2966.7	24.1
2887.8	0.1		2968.4	32.2
2889.6	0.5		2977.9	8.0

249

250

251

252

Conclusion and Future Plans

253 High resolution absorption cross sections of neopentane have been obtained in the 1200-1650 cm⁻¹
 254 region and cross sections in the 2550-3350 cm⁻¹ region have been recalculated. These cross
 255 sections are useful for the search of neopentane in the atmosphere of Titan, although lower
 256 temperatures (150-195 K) are desirable [5]. A local mode model for the CH stretching region has
 257 been presented and is in reasonable agreement with observations. As usual for hydrocarbons, the
 258 overtone and combination modes of the scissors vibrations are in Fermi resonance with the CH
 259 stretching modes. An unusual feature of neopentane is that a key scissor vibration is also in Fermi
 260 resonance with other lower frequency modes. A rotational analysis of the vibrational bands in the
 261 1200-1650 cm⁻¹ region is planned.

262 Acknowledgements

263 The NASA Outer Planets Research and Planetary Data Archiving and Restoration Tools program
 264 (PDART) provided funding (80NSSC19K0417). Part of the research described in this paper was
 265 performed at the Canadian Light Source, a national research facility of the University of
 266 Saskatchewan, which is supported by the Canada Foundation for Innovation (CFI), the Natural
 267 Sciences and Engineering Research Council (NSERC), the National Research Council (NRC), the
 268 Canadian Institutes of Health Research (CIHR), the Government of Saskatchewan, and the
 269 University of Saskatchewan. PB acknowledges productive discussions with RFB. ELS gratefully
 270 acknowledges support from NSF via Grant No. CHE-1900095.

271

272 **Supplementary materials:** The corrected Figures for [15] are available as supplementary
 273 materials. Because of their size, cross section data files are available from the MOLLIST website
 274 (<http://bernath.uwaterloo.ca/molecularlists.php>).

275

276 References

- 277 [1] Westbrook BR, Beasley GM, Fortenberry RC. Polycyclic aliphatic hydrocarbons: is
 278 tetrahedrane present in UIR spectra? *Phys Chem Chem Phys* 2022;24:14348.
 279 <https://doi.org/10.1039/d2cp01103d>
 280 [2] Pirali O, Boudon V, Oomens J, Vervloet M. Rotationally resolved infrared spectroscopy of
 281 adamantane. *J Chem Phys* 2012;136:024310. <https://doi.org/10.1063/1.3666853>

282 [3] Helmig D, Rossabi S, Hueber J, Tans P, Montzka SA, Masarie K, et al. Reversal of global
283 atmospheric ethane and propane trends largely due to US oil and natural gas production. *Nature*
284 *Geosci* 2016;9:490-495. <https://doi.org/10.1038/ngeo2721>

285 [4] Guerlet S, Fouchet T, Bézard B, Simon-Miller AA, Flasar FM. Vertical and meridional
286 distribution of ethane, acetylene and propane in Saturn's stratosphere from CIRS/Cassini limb
287 observations. *Icarus* 2009;203:214-32. <https://doi.org/10.1016/j.icarus.2009.04.002>

288 [5] Hörst, S. M. J. Titan's atmosphere and climate. *Geophys Res Planets* 2017;122:432-482.

289 [6] Loison JC, Dobrijevic M, Hickson KM. The photochemical production of aromatics in the
290 atmosphere of Titan. *Icarus* 2019;329:55-71. <https://doi.org/10.1016/j.icarus.2019.03.024>

291 [7] Rank DH., Saksena BD, Shull ER. Vibrational spectra of carbon and silicon tetramethyl and
292 their monodeutero derivatives. *Disc Faraday Soc* 1950;9:187-196.
293 <https://doi.org/10.1039/DF9500900187>

294 [8] Shull ER, Oakwood TS, Rank DH. Infrared and Raman spectra of tetramethylmethane-d₁₂. *J*
295 *Chem Phys* 1953;21:2024-2029. <https://doi.org/10.1063/1.1698736>

296 [9] Murata H, Shimizu K. Normal frequencies of tetramethylmethane. *J Chem Phys*
297 1957;27:599-600. <https://doi.org/10.1063/1.1743788>

298 [10] Sportouch S, Lacoste C, Gaufrès R. Spectres Raman du néopentane et du tétraméthylsilane
299 à l'état gazeux. *J Mol Struct* 1971;9:119-127. [https://doi.org/10.1016/0022-2860\(71\)85012-3](https://doi.org/10.1016/0022-2860(71)85012-3)

300 [11] Weiss S, Leroi GE. Infrared spectra and internal rotation in propane, isobutane and
301 neopentane. *Spectrochim Acta* 1969;25A:1759-1766. [https://doi.org/10.1016/0584-](https://doi.org/10.1016/0584-8539(69)80204-7)
302 [8539\(69\)80204-7](https://doi.org/10.1016/0584-8539(69)80204-7)

303 [12] Schachtscheider JH, Snyder RG. Vibrational analysis of the n-paraffins-II. Normal co-
304 ordinate calculations. *Spectrochim Acta* 1963;19:117-168. [https://doi.org/10.1016/0371-](https://doi.org/10.1016/0371-1951(63)80096-X)
305 [1951\(63\)80096-X](https://doi.org/10.1016/0371-1951(63)80096-X)

306 [13] Mirkin N, Krimm S. Ab initio analysis of the vibrational spectra of conformers of some
307 branched alkanes. *J Mol Struct* 2000;550-551:67-91. [https://doi.org/10.1016/S0022-](https://doi.org/10.1016/S0022-2860(00)00513-5)
308 [2860\(00\)00513-5](https://doi.org/10.1016/S0022-2860(00)00513-5)

309 [14] Bernath, PF, Sibert III EL, Dulick M. Neopentane Vibrations: High Resolution Spectra and
310 Anharmonic Calculations. *J Phys Chem A* 2020; DOI: 10.1021/acs.jpca.0c01723.

311 [15] Bernath P, Dodangodage R, Dulick M, Zhao J, Billinghurst B. Absorption cross sections for
312 neopentane broadened by nitrogen in the 3.3 micron region, *J Quant Spectrosc Rad Transfer*
313 2020;251:107034. DOI: 10.1016/j.jqsrt.2020.107034

314 [16] Hewett, D, Bernath P, Zhao J, Billinghurst B. Near infrared absorption cross sections for
315 ethane broadened by hydrogen and nitrogen. *J Quant Spectrosc Rad Transfer* 2020; 242:106780.
316 DOI: 10.1016/j.jqsrt.2019.106780

317 [17] Harrison JJ, Allen NDC, Bernath PF. Infrared absorption cross sections for ethane (C₂H₆) in
318 the 3 μm region. *J Quant Spectrosc Radiat Transfer* 2010;111:357-363.
319 <https://doi.org/10.1016/j.jqsrt.2009.09.010>

320 [18] Gordon IE, Rothman LS, Hargreaves RJ, Hashemi R, Karlovets E V., Skinner FM, et al.
321 The HITRAN2020 molecular spectroscopic database. *J Quant Spectrosc Radiat Transfer*
322 2022;277:107949. <https://doi.org/10.1016/j.jqsrt.2021.107949>.

323 [19] Bernath PF. MoLLIST: Molecular Line Lists, Intensities and Spectra. *J Quant Spectrosc*
324 *Rad Transfer* 2020;240:106687. DOI: 10.1016/j.jqsrt.2019.106687

325 [20] Bernath PF. *Spectra of Atoms and Molecules*, 4th edition. Oxford University Press, New
326 York, NY, 2020.

327 [21] Wenger C, Boudon V, Rotger M, Sanzharov M, Champion J-P. XTDS and SPVIEW:
328 Graphical tools for the analysis and simulation of high-resolution molecular spectra. J Mol
329 Spectrosc 2008;251:102-113. doi:10.1016/j.jms.2008.01.011
330 [22] Bernath PF, Bittner D, Sibert III, EL. Isobutane Infrared Bands: Partial Rotational
331 Assignments, Ab Initio Calculations and Local Mode Analysis. J Phys Chem A 2019;123:6185-
332 6193. DOI: 10.1021/acs.jpca.9b03321
333 [23] Tabor DP, Hewett DM, Bocklitz S, Korn JA, Tomaine AJ, Ghosh AK, Zwier TS, Sibert III
334 EL. Anharmonic modeling of the conformation-specific IR spectra of ethyl, *n*-propyl, and *n*-
335 butylbenzene. J Chem Phys 2016;144:224310. doi:10.1063/1.4953181
336 [24] Frisch MJ, Trucks GW, Schlegel HB, Scuseria GE, Robb MA, Cheeseman JR, et al.
337 Gaussian 09; Gaussian, Inc.: Wallingford CT, 2016.
338 [25] Raynes WT. Calculations of the force field of the methane molecule. Mol Phys
339 1987;60:509-525. doi:10.1080/00268978700100331
340
341
342
343